Torque Ripple Minimization of Predictive Current Control for IPMSMs with Improved Cost Function Design

Xiaofan Wang
School of Electrical Engineering
Beijing Jiaotong University
Beijing, China
xfwangs@bjtu.edu.cn

Xiaochun Fang
School of Electrical Engineering
Beijing Jiaotong University
Beijing, China
xcfang@bjtu.edu.cn

Zhi Wang
CRRC QingDao Sifang Rolling Stock Research Institute Co., Ltd.
Qingdao, China
wanna125246@163.com

Shuai Lin
School of Electrical Engineering
Beijing Jiaotong University
Beijing, China
17121459@bjtu.edu.cn

Fei Lin
School of Electrical Engineering
Beijing Jiaotong University
Beijing, China
flin@bjtu.edu.cn

Zhongping Yang
School of Electrical Engineering
Beijing Jiaotong University
Beijing, China
zhpyang@bjtu.edu.cn

***Abstract*—This paper applies model predictive current control (MPCC) to a typical 2-level voltage source inverter interior permanent magnet synchronous motor (VSI-IPMSM) rail vehicle drive system. However, simply controlling the current cannot minimize the torque ripple. An improved cost function design is proposed for VSI-IPMSM drives. The torque ripple information is integrated into the current error penalty function, so that the *d*-axis and *q*-axis current errors are reasonably distributed. The proposed cost function improves torque control accuracy at low sampling frequency and low switching frequency without adding torque and flux observer. The effectiveness of the proposed method has been verified by hardware-in-the-loop experiments.**

Keywords—Predictive current control, interior permanent magnet synchronous motor (IPMSM), torque ripple minimization, cost function, rail vehicle

I. INTRODUCTION

Now we are in an era of rapid development of rail transit technology. Due to the advantages of high efficiency, high power density and good torque characteristics, interior permanent magnet synchronous motor (IPMSM) is of great use in the traction system for high-speed railway and urban rail transit. In recent years, many advanced control technologies have been proposed to improve the control performance of IPMSM[1-6]. However, in practical applications, the classical linear control method with many limitations still occupies the mainstream.

The finite control set model predictive control (FCS-MPC) has advantages in multivariable and multi-target control without modulators and cascaded PI regulators, and is expected to grow into a future alternative to rail vehicle applications[7-18]. According to different control objectives, FCS-MPC can be divided into model predictive current control (MPCC)[7-10], model predictive torque control (MPTC)[7, 12-14] and model predictive speed control (MPSC)[15, 16]. Among them, in rail vehicle applications, the model required by MPSC is the most complicated and unnecessary, because the torque reference of the motor can be directly obtained from the traction control network. Compared to MPTC, MPCC does not require flux and torque estimation, which is simpler and more intuitionistic. Since communication, fault monitoring and protection in practical applications require a large computational burden, the sampling interval of the MPCC is relatively long (200 μs in this paper), which inevitably leads to current distortion and torque ripple.

Compared with the circular current boundary, the rectangular current boundary method can reduce the number of switches and help to realize the six-step operation[17, 18]. However, the ratio of length to width of rectangular boundary still lacks quantitative calculation basis. In this paper, on the premise of low switching frequency and small current distortion, and aiming at minimizing the torque ripple, we explore how to set the current boundary quantitatively.

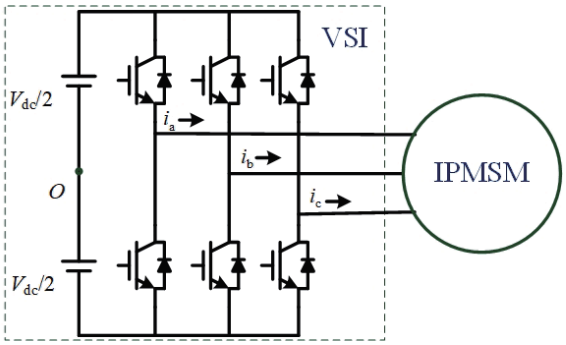

Fig. 1. The topology of 2-level VSI-IPMSM.

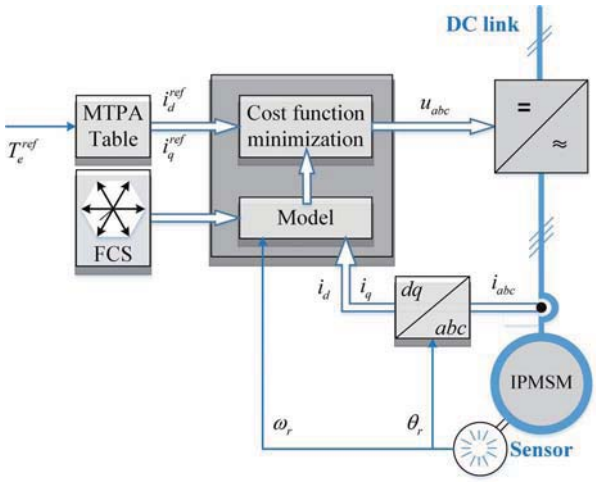

Fig. 2. MPCC diagram for IPMSM.

This work was supported by the Fundamental Research Funds for the Central Universities under Grant 2018YJS153.

The following chapters are arranged as follows: In section II, a 2-level VSI-IPMSM model is established and its MPCC implementation method is introduced. Then the proposed cost function design method is given. The torque ripple information is integrated into the current error penalty function, so that the *d*-axis and *q*-axis current errors are reasonably distributed. In section III, the effectiveness of the proposed method has been verified by hardware-in-the-loop experiments. The proposed cost function improves torque control accuracy at low sampling frequencies. Current distortion, torque ripple, switching frequency and other issues will be discussed in detail in this work. Section IV gives conclusions and possible research in the future.

II. Proposed Method for IPMSM Drives

A. MPCC for IPMSM Drives

In railway vehicles with induction motors, usually one inverter provides power for multiple motors. However, since the synchronous motors have no slip, in order to ensure the balance of output of all motors in the case of inconsistent wheel diameters, one inverter is generally used to supply power to one motor. A typical 2-level VSI-IPMSM rail train drive system is shown in Fig. 1.

Fig. 2 shows the control diagram used in this article. Typically, in applications such as rail transit and electric vehicles, torque reference T_e^{ref} is obtained from higher-level computers, so no speed loops are required. The reference of *d*-axis and *q*-axis currents (i_d^{ref} and i_q^{ref}) is obtained from a lookup table which is calculated by the maximum torque per ampere (MTPA) trajectory. The feedback channel contains the electric angular velocity ω_r, the electric angle θ_r and *d*-axis and *q*-axis currents (i_d and i_q) obtained by coordinate transformation.

The current predictive model after one beat delay compensation is (1)

$$\boldsymbol{i}^p(k+2)=\boldsymbol{A}\boldsymbol{i}(k+1)+\boldsymbol{B}\boldsymbol{u}(k+1)+\boldsymbol{C} \tag{1}$$

Where $x(k+1)$ represents the variable x corresponding to $k+1$, $x(k+2)$ represents the variable x corresponding to $k+2$, the superscript p represents the predicted value of the corresponding variable. The system matrix $\boldsymbol{A}$, the input matrix $\boldsymbol{B}$ and the back electromotive force $\boldsymbol{C}$ are as follows (2)

$$\begin{aligned}\boldsymbol{A}&=\begin{bmatrix}1-R_sT_s/L_d & L_qT_s\omega_r(k)/L_d\\ -L_dT_s\omega_r(k)/L_q & 1-R_sT_s/L_q\end{bmatrix}\\ \boldsymbol{B}&=\begin{bmatrix}T_s/L_d & 0\\ 0 & T_s/L_q\end{bmatrix}\\ \boldsymbol{C}&=\begin{bmatrix}0\\ -\psi_fT_s\omega_r(k)/L_q\end{bmatrix}\end{aligned} \tag{2}$$

In order to achieve current tracking control, the cost function can be defined as the distance between predictive currents and current references at time step $k+2$, which is shown in (3).

$$J_1=\sqrt{\left|i_d^{\,p}(k+2)-i_d^{\,ref}\right|^2+\left|i_q^{\,p}(k+2)-i_q^{\,ref}\right|^2} \tag{3}$$

Where i_d^{ref} and i_q^{ref} are considered to be constants from time step k to $k+2$.

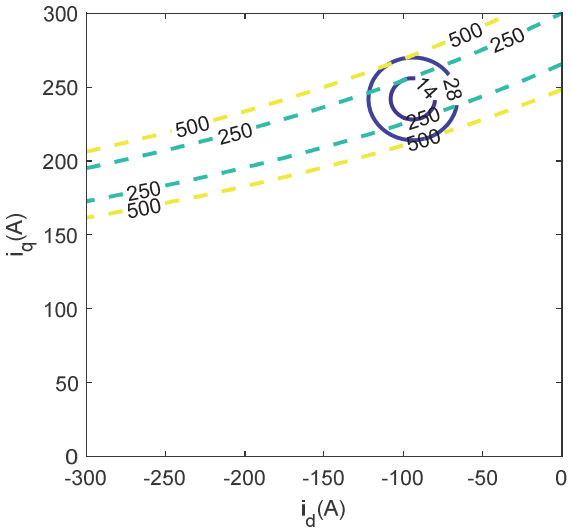

(a)

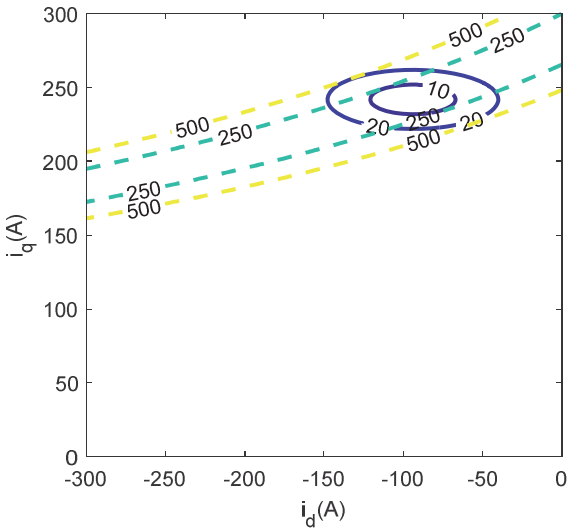

(b)

Fig. 3. Contour map of the current error term J_1, J_{1_Tmin} and torque error term ΔT_e. (a) J_1 and ΔT_e. (b) J_{1_Tmin} and ΔT_e.

B. Cost Function Design for Torque Ripple Minimization

The electromagnetic torque equation of IPMSM is (4)

$$\begin{aligned}T_e^{ref}&=\frac{3n_p}{2}\left[\psi_f+(L_d-L_q)i_d^{\,ref}\right]i_q^{\,ref}\\ T_e^{\,p}(k+2)&=\frac{3n_p}{2}\left[\psi_f+(L_d-L_q)i_d^{\,p}(k+2)\right]i_q^{\,p}(k+2)\end{aligned} \tag{4}$$

In this paper, the definition of torque ripple is based on the difference between the predicted value and the reference

value. According to (4), torque ripple ΔT_e can be expressed as (5)

$$\begin{aligned}\Delta T_e &= T_e^p(k+2) - T_e^{ref} \\ &= \frac{3n_p}{2}\left[\begin{array}{l}\psi_f \Delta i_q + \\ \left(L_d - L_q\right)\left(i_d^{ref}\Delta i_q + i_q^{ref}\Delta i_d + \Delta i_d \Delta i_q\right)\end{array}\right]\end{aligned} \quad (5)$$

Where $\Delta i_d = i_d^p(k+2) - i_d^{ref}$ and $\Delta i_d = i_q^p(k+2) - i_q^{ref}$. In most cases, the term $\Delta i_d \Delta i_q$ is relatively small. If this term is ignored, we can get

$$\begin{aligned}\Delta T_e \approx & \frac{3n_p}{2}\left(L_d - L_q\right) i_q^{ref} \Delta i_d \\ & + \frac{3n_p}{2}\left[\psi_f + \left(L_d - L_q\right) i_d^{ref}\right] \Delta i_q\end{aligned} \quad (6)$$

The weights of the *d*-axis and *q*-axis current errors in the torque ripple are

$$\begin{aligned}\lambda_d &= \left|\left(L_d - L_q\right) i_q^{ref}\right| \\ \lambda_q &= \left|\psi_f + \left(L_d - L_q\right) i_d^{ref}\right|\end{aligned} \quad (7)$$

Based on (3) and (7), in order to minimize the torque ripple, the proposed cost function containing current error distribution weights is

$$J_{I\_T\min} = \sqrt{\begin{array}{l}\dfrac{\lambda_d^2}{\lambda_q^2}\left|i_d^p(k+2) - i_d^{ref}\right|^2 \\ + \left|i_q^p(k+2) - i_q^{ref}\right|^2\end{array}} \quad (8)$$

C. Analysis and Comparison of the Cost Functions

Fig. 3 shows the contour map of the cost function J_I, $J_{I\_T\min}$ and torque error term ΔT_e in *d*-*q* plane. We can see that the proposed cost function $J_{I\_T\min}$ turns the contour from circles into ellipses. That is to say, the adjustment capability of the *q*-axis current is enhanced.

III. Experimental Results

A. Test Platform

The experimental platform is shown in Fig. 4. This platform has successfully supported the development of various types of rail vehicle traction systems in China. And it has been fully validated for the simulation of actual vehicle traction systems.

Table I shows the PMSM parameters and rated values. The model of the motor and load runs in the dSPACE platform. The controller is a traction control unit (TCU) which was designed for metro vehicles. The TCU adopts DSP+FPGA hardware control architecture. It has peripherals including photoelectric conversion module, ADC module, digital I/O module, flash memory device, communication module, and so on. The FCS-MPC algorithm is implemented by DSP (TMS320C6748). Sampling and driving pulses are performed by the FPGA. A HIOKI 8860-50 Memory Hicorder is used to save the sample and control data. In this work, the sampling interval T_s is set to be 200 μs (5kHz).

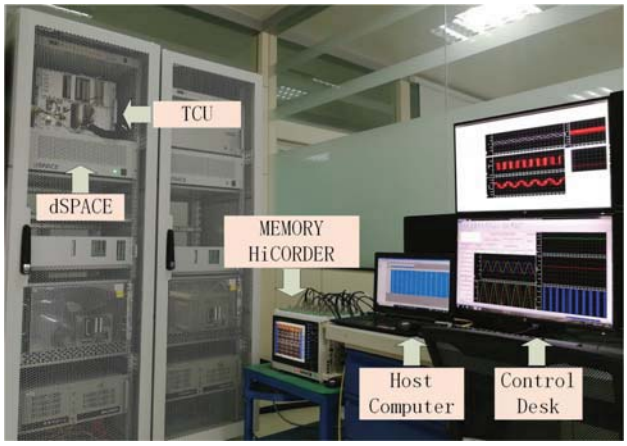

Fig. 4. The experimental platform.

TABLE I
THE PMSM PARAMETERS

Parameters	Values
Dc-link voltage (V)	750
Maximum power (kW)	254
Maximum speed (rpm)	550
Maximum torque (Nm)	5669
Maximum current (A)	329
Pole pairs	8
R_s (mΩ)	91.8
L_d (mH)	2.6
L_q (mH)	4.7
ψ_f (Wb)	1.2081

TABLE II
PERFORMANCE EVALUATION (when i_d^{ref} = -95A, i_q^{ref} = 238A)

Variables	With J_I	With $J_{I\_T\min}$
Current ripple in *d*-axis Δi_d (A)	34.1	48.4
Current ripple in *q*-axis Δi_q (A)	33.2	20.4
Torque ripple ΔT_e (Nm)	536	380
Switching frequency (Hz)	738	743

B. Performance Evaluation

First, the motor is dragged by a large inertia load to run steadily at a fixed speed. Fig. 5 shows the comparison of *d*-axis and *q*-axis current, torque, and phase current at the speed of 150rpm. The given order of torque instruction is (idling → 100% traction → 100% braking → idling). It can be seen that the proposed cost function can significantly reduce the *q*-axis current ripple and torque ripple. Fig.6 shows the results with same torque instruction at 300rpm. Similarly, the proposed method reduces the *q*-axis current ripple and torque ripple. However, it should be pointed out that *d*-axis ripple in Fig.5 and Fig.6 increases after using the proposed method, because the weight factor of *d*-axis error decreases.

Table II shows the value of current ripple, torque ripple, and switching frequency when the motor is operating at i_d^{ref} = -95A, i_q^{ref} = 238A. The torque ripple of the proposed

method is reduced by 29% (from 536 to 380 Nm) compared to the conventional method. In addition, the switching frequency of the two methods is basically the same.

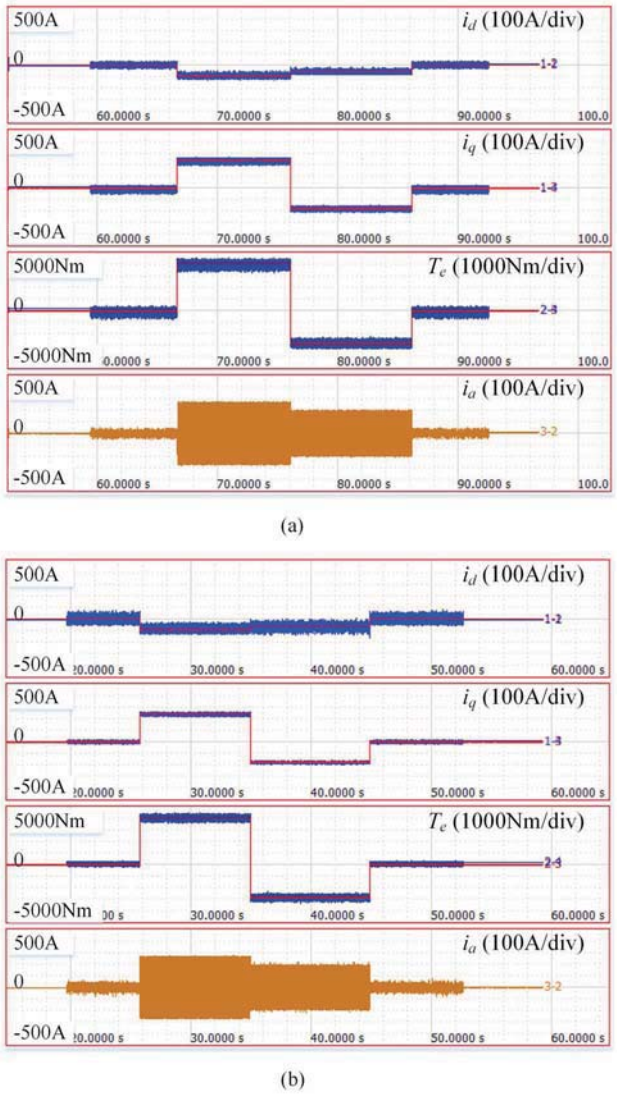

Fig. 5. Comparison of i_d, i_q, T_e, and i_a. (a) With the cost function J_I. (b) With the proposed cost function J_{I_Tmin}.

Fig. 7 shows the FFT analysis of the phase current i_a, when the motor is operating at i_d^{ref} = -95A, i_q^{ref} = 238A. The current THD of the traditional method is 7.33%, while the current THD of the proposed method is 7.36%. They are almost the same. It can be seen that the proposed method does not make the current distortion serious. Fig. 8 shows the current trajectories of the two methods at the steady-state operation points mentioned above. The duration of the data in Fig. 8 is 0.3s. It can be seen that the boundary of the current in the traditional method is approximately a circle. In the proposed method, the current boundary becomes an ellipse, which has a wide range in the direction of d-axis and a narrow range in the direction of q- axis.

Fig. 9 is an enlarged view of step response from idling to 100% traction operation. We can see that the effect of modifying the cost function on the dynamic response is negligible. The dynamic process is very fast (about 5ms) and there is no overshoot.

Fig. 10 shows the experimental results under varying speed conditions. Firstly, 100% traction torque was given in the static state to accelerate the motor to 300rpm.Then given 100% brake torque, the motor deceleration to 0. Due to the large inertia load (railway vehicles), the process of acceleration and deceleration is slow. It can be seen that the proposed method has effectively reduced the torque ripple in the whole speed range, as well as the q-axis current ripple.

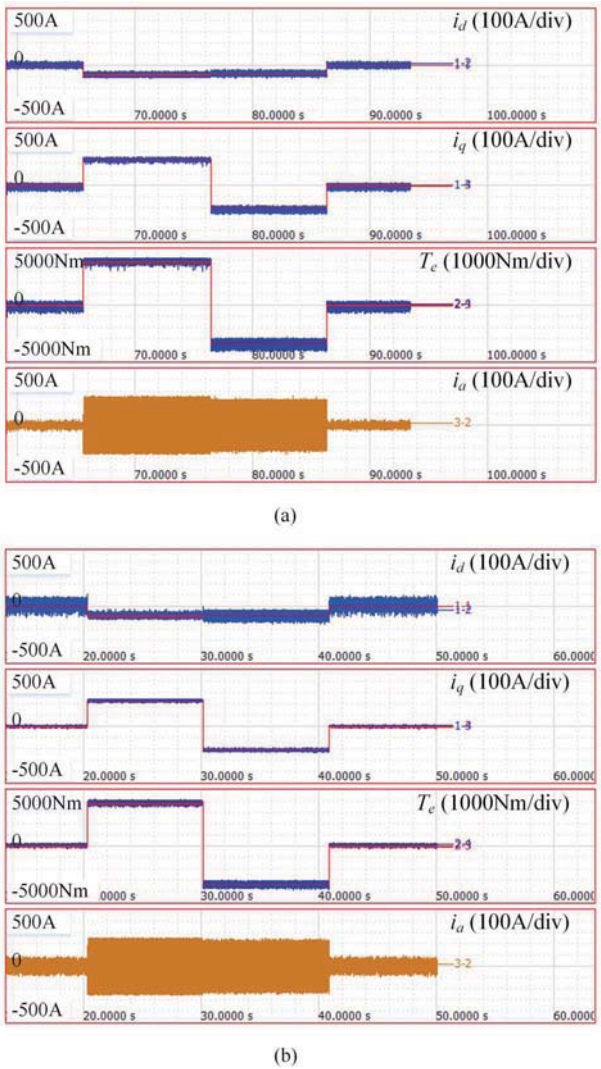

Fig. 6. Comparison of i_d, i_q, T_e, and i_a. (a) With the cost function J_I. (b) With the proposed cost function J_{I_Tmin}.

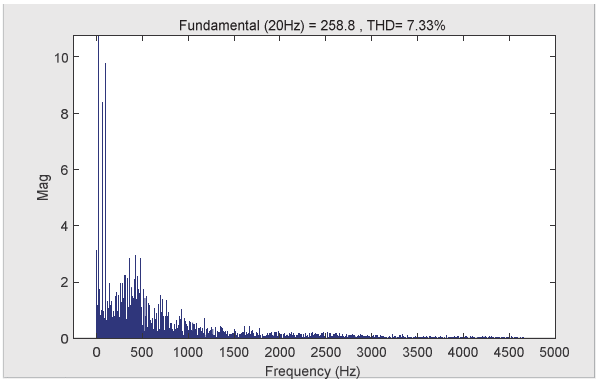

(a)

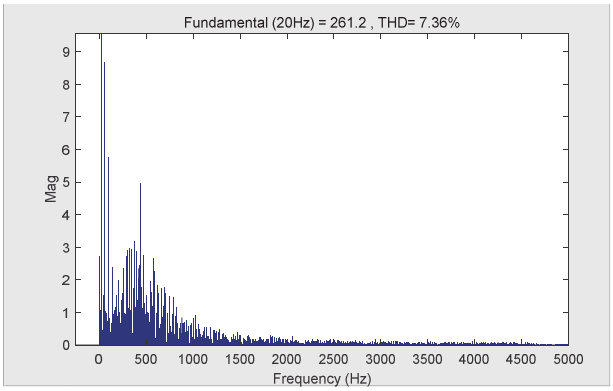

(b)

Fig. 7. FFT analysis of the phase current i_a, when the motor is operating at i_d^{ref} = -95A, i_q^{ref} = 238A. (a) With the cost function J_I. (b) With the proposed cost function J_{I_Tmin}.

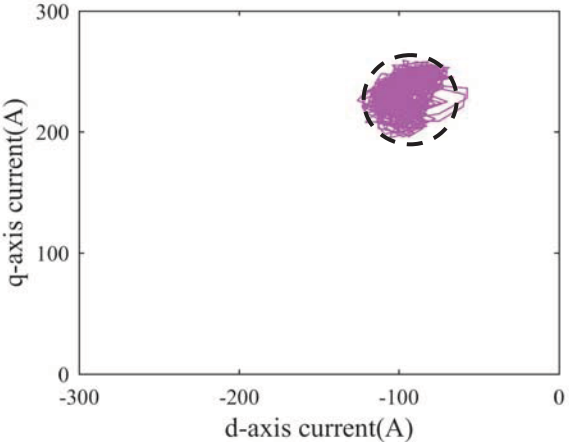

(a)

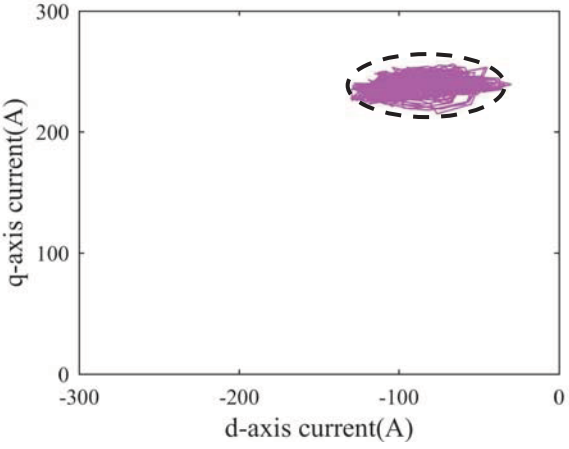

(b)

Fig. 8. Comparison of current trajectories at steady state when the motor is operating at i_d^{ref} = -95A, i_q^{ref} = 238A. (a) With the cost function J_I. (b) With the proposed cost function J_{I_Tmin}.

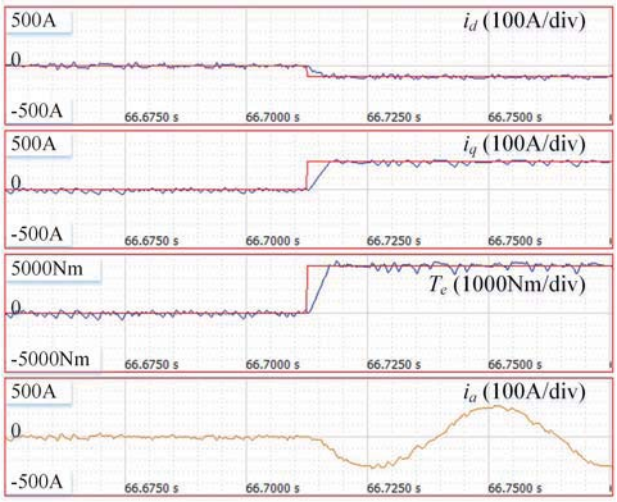

(a)

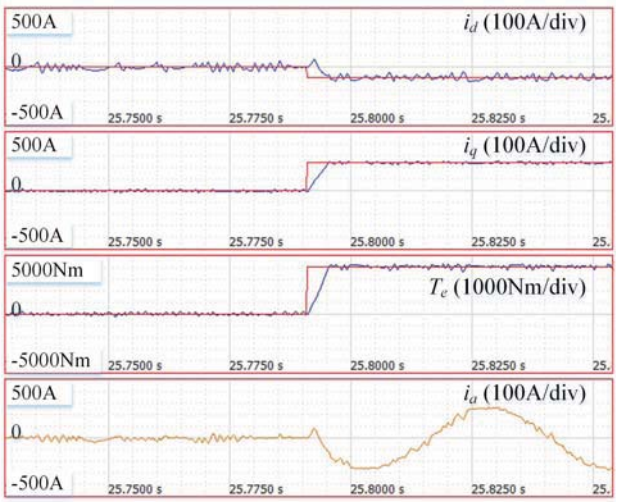

(b)

Fig. 9. Dynamic processes of step response. (a) With the cost function J_I. (b) With the proposed cost function J_{I_Tmin}.

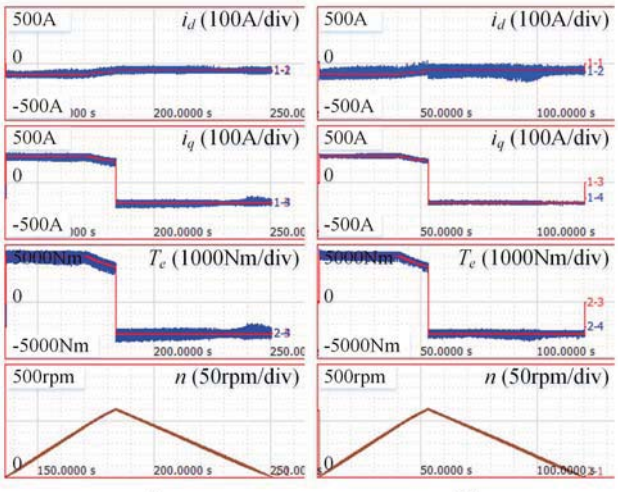

(a) (b)

Fig. 10. Comparison of i_d, i_q, and T_e when speed varing. (a) With the cost function J_I. (b) With the proposed cost function J_{I_Tmin}.

IV. Conclusion

Based on the VSI-IPMSM drive system using MPCC, this paper proposes an improved cost function design method. The proposed method does not need to add any torque and flux observer, nor modify the prediction model, making full use of the simple and intuitive advantages of MPCC. Experiments show that the proposed method can effectively reduce the torque ripple (29%) at steady state, while the switching frequency and dynamic response of the system are almost unaffected.

Due to the reduced *d*-axis current weight in the proposed cost function, the *d*-axis current ripple increases, which will lead to a decrease in control performance, especially in the flux-weakening region. In future research, we will try to find a cost function design method suitable for flux-weakening region.

References

[1] F. Betin et al., "Trends in Electrical Machines Control: Samples for Classical, Sensorless, and Fault-Tolerant Techniques," IEEE Industrial Electronics Magazine, vol. 8, no. 2, pp. 43-55, 2014.

[2] M. P. Kazmierkowski, L. G. Franquelo, J. Rodriguez, M. A. Perez, and J. I. Leon, "High-Performance Motor Drives," IEEE Industrial Electronics Magazine, vol. 5, no. 3, pp. 6-26, 2011.

[3] M. N. Uddin and M. M. Rahman, "Online Torque-Flux Estimation-Based Nonlinear Torque and Flux Control Scheme of IPMSM Drive for Reduced Torque Ripples," IEEE Transactions on Power Electronics, vol. 34, no. 1, pp. 636-645, 2019.

[4] N. Zhao, G. Wang, D. Xu, L. Zhu, G. Zhang, and J. Huo, "Inverter Power Control Based on DC-Link Voltage Regulation for IPMSM Drives Without Electrolytic Capacitors," IEEE Transactions on Power Electronics, vol. 33, no. 1, pp. 558-571, 2018.

[5] G. Wang, R. Liu, N. Zhao, D. Ding, and D. Xu, "Enhanced Linear ADRC Strategy for HF Pulse Voltage Signal Injection-Based Sensorless IPMSM Drives," IEEE Transactions on Power Electronics, vol. 34, no. 1, pp. 514-525, 2019.

[6] Z. Zhang, C. Wang, M. Zhou, and X. You, "Flux-Weakening in PMSM Drives: Analysis of Voltage Angle Control and the Single Current Controller Design," IEEE Journal of Emerging and Selected Topics in Power Electronics, vol. 7, no. 1, pp. 437-445, 2019.

[7] J. Scoltock, T. Geyer, and U. K. Madawala, "A Comparison of Model Predictive Control Schemes for MV Induction Motor Drives," IEEE Transactions on Industrial Informatics, vol. 9, no. 2, pp. 909-919, 2013.

[8] M. Siami, D. A. Khaburi, M. Rivera, and J. Rodríguez, "An Experimental Evaluation of Predictive Current Control and Predictive Torque Control for a PMSM Fed by a Matrix Converter," IEEE Transactions on Industrial Electronics, vol. 64, no. 11, pp. 8459-8471, 2017.

[9] W. Wang, Y. Fan, S. Chen, and Q. Zhang, "Finite control set model predictive current control of a five-phase PMSM with virtual voltage vectors and adaptive control set," CES Transactions on Electrical Machines and Systems, vol. 2, no. 1, pp. 136-141, 2018.

[10] Y. Zhang, L. Huang, D. Xu, J. Liu, and J. Jin, "Performance evaluation of two-vector-based model predictive current control of PMSM drives," Chinese Journal of Electrical Engineering, vol. 4, no. 2, pp. 65-81, 2018.

[11] S. Vazquez, J. Rodriguez, M. Rivera, L. G. Franquelo, and M. Norambuena, "Model Predictive Control for Power Converters and Drives: Advances and Trends," IEEE Transactions on Industrial Electronics, vol. 64, no. 2, pp. 935-947, 2017.

[12] M. Preindl and S. Bolognani, "Model Predictive Direct Torque Control With Finite Control Set for PMSM Drive Systems, Part 1: Maximum Torque Per Ampere Operation," IEEE Transactions on Industrial Informatics, vol. 9, no. 4, pp. 1912-1921, 2013.

[13] Z. Zhou, C. Xia, Y. Yan, Z. Wang, and T. Shi, "Torque Ripple Minimization of Predictive Torque Control for PMSM With Extended Control Set," IEEE Transactions on Industrial Electronics, vol. 64, no. 9, pp. 6930-6939, 2017.

[14] M. Preindl and S. Bolognani, "Model Predictive Direct Torque Control With Finite Control Set for PMSM Drive Systems, Part 2: Field Weakening Operation," IEEE Transactions on Industrial Informatics, vol. 9, no. 2, pp. 648-657, 2013.

[15] M. Preindl and S. Bolognani, "Model Predictive Direct Speed Control with Finite Control Set of PMSM Drive Systems," IEEE Transactions on Power Electronics, vol. 28, no. 2, pp. 1007-1015, 2013.

[16] P. Kakosimos and H. Abu-Rub, "Predictive Speed Control With Short Prediction Horizon for Permanent Magnet Synchronous Motor Drives," IEEE Transactions on Power Electronics, vol. 33, no. 3, pp. 2740-2750, 2018.

[17] J. Holtz, "Advanced PWM and Predictive Control—An Overview," IEEE Transactions on Industrial Electronics, vol. 63, no. 6, pp. 3837-3844, 2016.

[18] A. Khambadkone and J. Holtz, "Low switching frequency and high dynamic pulsewidth modulation based on field-orientation for high-power inverter drive," IEEE Transactions on Power Electronics, vol. 7, no. 4, pp. 627-632, 1992.